

## A direct numerical simulation study of vorticity transformation in weakly turbulent premixed flames

A. N. Lipatnikov,<sup>1,a)</sup> S. Nishiki,<sup>2</sup> and T. Hasegawa<sup>3</sup>

<sup>1</sup>*Department of Applied Mechanics, Chalmers University of Technology, Gothenburg 412 96, Sweden*

<sup>2</sup>*Department of Mechanical Engineering, Kagoshima University, Kagoshima 890-0065, Japan*

<sup>3</sup>*EcoTopia Science Institute, Nagoya University, Nagoya 464-8603, Japan*

(Received 28 May 2014; accepted 6 October 2014; published online 22 October 2014)

Database obtained earlier in 3D Direct Numerical Simulations (DNS) of statistically stationary, 1D, planar turbulent flames characterized by three different density ratios  $\sigma$  is processed in order to investigate vorticity transformation in premixed combustion under conditions of moderately weak turbulence (rms turbulent velocity and laminar flame speed are roughly equal to one another). In cases H and M characterized by  $\sigma = 7.53$  and 5.0, respectively, anisotropic generation of vorticity within the flame brush is reported. In order to study physical mechanisms that control this phenomenon, various terms in vorticity and enstrophy balance equations are analyzed, with both mean terms and terms conditioned on a particular value  $c$  of the combustion progress variable being addressed. Results indicate an important role played by baroclinic torque and dilatation in transformation of average vorticity and enstrophy within both flamelets and flame brush. Besides these widely recognized physical mechanisms, two other effects are documented. First, viscous stresses redistribute enstrophy within flamelets, but play a minor role in the balance of the mean enstrophy  $\overline{\Omega}$  within turbulent flame brush. Second, negative correlation  $\overline{\mathbf{u}' \cdot \nabla \Omega'}$  between fluctuations in velocity  $\mathbf{u}$  and enstrophy gradient contributes substantially to an increase in the mean  $\overline{\Omega}$  within turbulent flame brush. This negative correlation is mainly controlled by the positive correlation between fluctuations in the enstrophy and dilatation and, therefore, dilatation fluctuations substantially reduce the damping effect of the mean dilatation on the vorticity and enstrophy fields. In case L characterized by  $\sigma = 2.5$ , these effects are weakly pronounced and  $\overline{\Omega}$  is reduced mainly due to viscosity. Under conditions of the present DNS, vortex stretching plays a minor role in the balance of vorticity and enstrophy within turbulent flame brush in all three cases. © 2014 AIP Publishing LLC. [<http://dx.doi.org/10.1063/1.4898640>]

### I. INTRODUCTION

When a premixed flame propagates in a turbulent flow, not only the turbulence affects the flame by wrinkling its surface, increasing the mean burning rate, and flame brush thickness,<sup>1–3</sup> but also heat release and density variations in the flame can substantially affect the flow field. Although manifestations of the latter effects such as the hydrodynamic Darrieus-Landau (DL) instability of a premixed flame<sup>4</sup> or so-called flame-generated turbulence<sup>5</sup> have been known for a long time, capabilities of contemporary models of premixed burning for predicting the influence of combustion on turbulence are still poor, as reviewed in Ref. 6, with the focus of such models being placed on flow characteristics that are mainly controlled by large-scale eddies, e.g., the rms turbulent velocity  $u'$ , mean turbulent kinetic energy  $\bar{k}$ , or turbulent scalar flux. The influence of combustion on flow

<sup>a)</sup>Electronic mail: [lipatn@chalmers.se](mailto:lipatn@chalmers.se).

characteristics that are significantly affected by small-scale turbulent eddies has yet drawn much less attention in spite of substantial importance of the latter quantities for modeling the influence of turbulence on premixed flames.

Indeed, the primary physical mechanism of an increase in burning rate by turbulence consists of stretching of the flame surface by turbulent eddies,<sup>1-3</sup> with the highest local stretch rates being produced by the smallest eddies, at least within the framework of the Kolmogorov paradigm. In a premixed flame brush, the efficiency of the smallest eddies in stretching the flame surface is reduced due to dilatation and viscous dissipation in the preheat zone of the flame front,<sup>7,8</sup> but efficient larger-scale eddies can still be substantially smaller than eddies that control  $u'$  or  $\bar{k}$ . Therefore, the influence of heat release on (moderately) small-scale eddies should be properly addressed in order to model the effect of that eddies on the flame surface. In the isotropic Kolmogorov turbulence, such eddies are characterized by their length scale and the mean dissipation rate  $\bar{\epsilon}$ , which is approximately equal to  $2\nu\bar{\Omega}$ . Here,  $\Omega = \boldsymbol{\omega}' \cdot \boldsymbol{\omega}'/2$  is enstrophy,  $\boldsymbol{\omega} = \nabla \times \mathbf{u}$  and  $\mathbf{u}$  are vorticity and velocity vectors, respectively, and  $\nu$  is the kinematic viscosity of the fluid. Accordingly, the vorticity and enstrophy are important characteristics of small-scale turbulent eddies, at least in constant-density flows.

Moreover, within a premixed flame brush, characterization of turbulence is an issue due to intermittency<sup>9</sup> of cold, heavy unburned gas, and hot, light combustion products separated by a thin wrinkled flame front. For instance, if the probability  $\gamma$  of finding intermediate (between unburned and burned) states of the mixture is much less than unity, then, the standard Reynolds stresses

$$\overline{\rho u'_i u'_j} = \bar{\rho}(1 - \bar{c})(\overline{u'_i u'_j})_u + \bar{\rho}\bar{c}(\overline{u'_i u'_j})_b + \bar{\rho}\bar{c}(1 - \bar{c})(\bar{u}_{i,b} - \bar{u}_{i,u})(\bar{u}_{j,b} - \bar{u}_{j,u}) \quad (1)$$

are controlled not only by turbulence, but also by the flame-induced slip velocity<sup>10</sup>  $\Delta \mathbf{u} \equiv \bar{\mathbf{u}}_b - \bar{\mathbf{u}}_u$ , with  $\Delta \mathbf{u}$  dominating in weakly turbulent flames. Here,  $\rho$  is the density,  $c$  is the combustion progress variable,<sup>11</sup>  $\bar{\mathbf{u}}_u$  and  $\bar{\mathbf{u}}_b$  are velocity vectors conditioned on unburned ( $c = 0$ ) and burned ( $c = 1$ ) mixture, respectively, overlines and overbars designate Reynolds-averaging with  $q' \equiv q - \bar{q}$ , while  $\bar{q} \equiv \overline{\rho q}/\bar{\rho}$  is the Favre-averaged (mass weighted) value of a quantity  $q$  with  $q'' \equiv q - \bar{q}$ , and subscripts  $u$  and  $b$  designate unburned and burned gas, respectively.

Because turbulence and the combustion-induced slip velocity are totally different phenomena, the use of the standard Reynolds stresses or any rms velocity based on them, e.g.,  $(\overline{u'_k u'_k})^{1/2}/3$  or  $(\overline{u'_1 u'_1})^{1/2}$ , does not seem to be a basically justified approach to characterizing turbulence within a premixed turbulent flame brush. A widely accepted way to resolving the problem consisted of considering the conditioned Reynolds stresses  $(\overline{u'_i u'_j})_u$  and  $(\overline{u'_i u'_j})_b$  to be the true turbulence characteristics. However, the validity of using  $(\overline{u'_i u'_j})_u$  and  $(\overline{u'_i u'_j})_b$  to characterize turbulence was put into question by showing substantial difference in  $\overline{u'_i u'_j}$  and the conditioned Reynolds stresses in constant-density reacting flows.<sup>12,13</sup> Even if chemical reactions do not affect turbulence in the case of a constant density, conditional averaging of a field  $q(\mathbf{x}, t)$  over a spatial region bounded by a moving interface (the reaction front) yields result that can be substantially different<sup>14</sup> from the Reynolds-averaged  $\bar{q}(\mathbf{x}, t)$ .

While the problem of characterizing turbulence within a premixed flame brush has not yet been resolved, it is tempting to assume that quantities that are controlled by the gradients of the velocity field, i.e., by small-scale eddies, are less sensitive to conditional averaging than the Reynolds stresses, which are significantly affected by large-scale eddies. This assumption was confirmed in a recent Direct Numerical Simulation (DNS) study of a self-propagating interface in 3D isotropic, constant-density turbulence.<sup>15</sup> In particular, it was shown that the conditioned and Reynolds-averaged enstrophies were close to each other in all simulated cases, whereas the conditioned  $(\overline{u'_i u'_j})_u$  and  $(\overline{u'_i u'_j})_b$  differed significantly from the canonical  $\overline{u'_i u'_j}$ . Accordingly, conditioned enstrophy appears to be a better turbulence characteristic than conditioned Reynolds stresses and, therefore, enstrophy transformation in flames is worth studying.

The above reasoning implies that investigation of the evolution of small-scale turbulence characteristics such as enstrophy, vorticity, etc., under the influence of combustion-induced heat release and density variations is of substantial importance for both general understanding and development of predictive models of premixed turbulent burning. For a long time, such investigations were very limited, as reviewed in Ref. 6. Over past years, target-directed research into the issue was started

thanks to development of advanced measurement and numerical tools such as cinema-stereoscopic PIV and DNS, respectively. For instance, Steinberg *et al.*<sup>16–19</sup> reported results of an exhaustive experimental study of vorticity fields in rim-stabilized premixed turbulent flames.

In the DNS literature, a number of images of instantaneous vorticity fields can be found,<sup>20–30</sup> with a few recent DNS papers<sup>31–34</sup> aiming at quantitatively investigating vorticity changes due to premixed turbulent combustion. In particular, Treurniet *et al.*<sup>31</sup> simulated weakly and moderately turbulent premixed flames characterized by various density ratios  $\sigma$  and documented anisotropic generation of vorticity in the cases of  $\sigma = 6$  or  $4$ , whereas the computed vorticity decayed within turbulent flame brush in the case of a lower density ratio, i.e.,  $\sigma = 2$ . Hamlington *et al.*<sup>32,33</sup> also reported that combustion made vorticity field anisotropic, but the computed magnitude of vorticity vector decayed within premixed turbulent flame brushes in all cases simulated by them. This difference between the results obtained by Treurniet *et al.*<sup>31</sup> and Hamlington *et al.*<sup>32,33</sup> will further be discussed in the beginning of Sec. IV A. Chakraborty<sup>34</sup> investigated statistics of vorticity alignment with local strain rates and found the predominant alignment of vorticity vector with the intermediate principal strain rate in various premixed turbulent flames simulated by him.

The goal of the present work is to analyze DNS data in order to gain further insight into the influence of premixed combustion on the transformation of vorticity and enstrophy in a turbulent flow.

In Sec. II, balance equations for  $\omega$  and  $\Omega$  and physical mechanisms that control vorticity transformation in flames are summarized. DNS attributes are discussed in Sec. III. Numerical results are analyzed in Sec. IV followed by conclusions.

## II. BACKGROUND

The following vorticity balance equation

$$\frac{\partial \omega_i}{\partial t} + u_k \frac{\partial \omega_i}{\partial x_k} = \underbrace{\omega_k \frac{\partial u_i}{\partial x_k}}_1 + \underbrace{\epsilon_{ijk} \frac{\partial}{\partial x_j} \left( \frac{1}{\rho} \frac{\partial \tau_{kl}}{\partial x_l} \right)}_2 - \underbrace{\omega_i \frac{\partial u_k}{\partial x_k}}_3 + \underbrace{\frac{1}{\rho^2} \epsilon_{ijk} \frac{\partial \rho}{\partial x_j} \frac{\partial p}{\partial x_k}}_4 \quad (2)$$

can be derived by taking the curl of Navier-Stokes equation. Here,  $t$  is the time,  $x_i$  are spatial coordinates,  $\omega_i$  and  $u_i$  are components of the vorticity and velocity vectors, respectively,  $p$  is the pressure,

$$\tau_{ij} = \rho \nu \left( \frac{\partial u_i}{\partial x_j} + \frac{\partial u_j}{\partial x_i} - \frac{2}{3} \delta_{ij} \frac{\partial u_k}{\partial x_k} \right) \quad (3)$$

is the viscous stress tensor,  $\delta_{ij}$  is the Kronecker delta,  $\epsilon_{ijk}$  is the cyclic permutation tensor, and the summation convention applies for the repeated indexes  $k$  and  $l$ .

In constant-density case, Eq. (2) reads

$$\frac{\partial \omega_i}{\partial t} + u_k \frac{\partial \omega_i}{\partial x_k} = \underbrace{\omega_k \frac{\partial u_i}{\partial x_k}}_{1'} + \underbrace{\nu \frac{\partial^2 \omega_i}{\partial x_k^2}}_{2'}. \quad (4)$$

In a turbulent flow, terms 1' and 2' are associated with vorticity generation due to vortex stretching and viscous redistribution, respectively.

A flame affects terms 1 and 2 by changing the velocity field and, moreover, term 2 subsumes subterms, which involve derivatives of the density and viscosity. Dilatation term 3 and baroclinic torque term 4 on the Right-Hand Side (RHS) of Eq. (2) are specific to variable density flows. The dilatation term always decreases vorticity, whereas the baroclinic torque can either increase or damp vorticity depending on the angle between vectors  $\nabla \rho \times \nabla p$  and  $\omega$ .

Equation (2) can be rewritten as follows

$$\frac{\partial}{\partial t} \left( \frac{\omega_i}{\rho} \right) + u_k \frac{\partial}{\partial x_k} \left( \frac{\omega_i}{\rho} \right) = \frac{1}{\rho} \left[ \omega_k \frac{\partial u_i}{\partial x_k} + \epsilon_{ijk} \frac{\partial}{\partial x_j} \left( \frac{1}{\rho} \frac{\partial \tau_{kl}}{\partial x_l} \right) + \frac{1}{\rho^2} \epsilon_{ijk} \frac{\partial \rho}{\partial x_j} \frac{\partial p}{\partial x_k} \right] \quad (5)$$

using the continuity equation and moving the dilatation term from the RHS to the Left-Hand Side (LHS). Application of Eq. (5) to a 2D steady inviscid flow yields

$$u_k \frac{\partial}{\partial x_k} \left( \frac{\omega_3}{\rho} \right) = -\frac{1}{\rho} \varepsilon_{3jk} \frac{\partial}{\partial x_j} \left( \frac{1}{\rho} \right) \frac{\partial p}{\partial x_k}, \quad (6)$$

thus, highlighting the baroclinic torque to be the sole physical mechanism that can overwhelm the expansion of hot products and can produce vorticity in a flame. In order for this mechanism to play a role, misalignment of the vectors  $\nabla \rho$  and  $\nabla p$  is necessary.

In the same simple case, the following relation

$$\rho_u S_L (\omega_{3,b} - \omega_{3,u}) = \frac{\rho_u - \rho_b}{2} \frac{\partial u_t^2}{\partial \mu} \quad (7)$$

can be derived<sup>35</sup> for the jump in the vorticity component  $\omega_3$  at a laminar flame provided that  $\rho u_n$  and  $p + \rho u_n^2$  do not change in the flame along the normal to it and the laminar flame speed  $S_L$  is constant. Here,  $u_n$  and  $u_t$  are the components of the velocity vector that are locally normal and tangential, respectively, to the flame,  $\mu$  is the locally tangential coordinate in the  $xy$ -plane. Equations (6) and (7) link the baroclinic torque and the strain rate  $\partial u_t / \partial \mu$ . The baroclinic torque can generate vorticity only due to the tangential pressure gradient, which causes tangential variations in  $u_t$ .

If the mean flow is irrotational and  $\bar{\omega} = 0$ , then,  $\Omega = \omega \cdot \omega / 2$  and a balance equation for the enstrophy can be obtained by multiplying Eq. (2) with  $\omega_i$ , i.e.,

$$\frac{\partial \Omega}{\partial t} + u_k \frac{\partial \Omega}{\partial x_k} = \underbrace{\omega_i \omega_k \frac{\partial u_i}{\partial x_k}}_{T_1} - \underbrace{\frac{\varepsilon_{ijk} \omega_i}{\rho^2} \frac{\partial \rho}{\partial x_j} \frac{\partial \tau_{kl}}{\partial x_l}}_{T_{21}} + \underbrace{\frac{\varepsilon_{ijk} \omega_i}{\rho} \frac{\partial^2 \tau_{kl}}{\partial x_l \partial x_j}}_{T_{22}} - \underbrace{2\Omega \frac{\partial u_k}{\partial x_k}}_{T_3} + \underbrace{\frac{\varepsilon_{ijk} \omega_i}{\rho^2} \frac{\partial \rho}{\partial x_j} \frac{\partial p}{\partial x_k}}_{T_4}. \quad (8)$$

In the statistically stationary planar 1D case, the Reynolds-averaged equation is as follows:

$$\overline{u_k \frac{\partial \Omega}{\partial x_k}} = \underbrace{\overline{\omega_i \omega_k \frac{\partial u_i}{\partial x_k}}}_I + \underbrace{\overline{\varepsilon_{ijk} \omega_i \frac{\partial}{\partial x_j} \left( \frac{1}{\rho} \frac{\partial \tau_{kl}}{\partial x_l} \right)}}_{II} - \underbrace{\overline{2\Omega \frac{\partial u_k}{\partial x_k}}}_{III} + \underbrace{\overline{\varepsilon_{ijk} \frac{1}{\rho^2} \omega_i \frac{\partial \rho}{\partial x_j} \frac{\partial p}{\partial x_k}}}_{IV}. \quad (9)$$

In the following, various terms on the RHSs of Eqs. (2), (8), and (9) will be evaluated by processing DNS data obtained earlier by Nishiki *et al.*<sup>28,36</sup> Equation (2) is selected among two equivalent equations (2) and (5), because the RHS of the latter equation does not allow us to address the dilatation effects straightforwardly. It is also worth noting that while the Favre-averaged dissipation rate is invoked by various models of premixed turbulent combustion, this fact does not necessitate that the Favre-averaged enstrophy is more suitable for incorporating into those models when compared to the Reynolds-averaged  $\bar{\Omega}$ . Indeed, averaging of  $\varepsilon = 2\nu\Omega$  results neither in  $\bar{\varepsilon} = 2\bar{\nu}\bar{\Omega}$  nor in  $\bar{\varepsilon} = 2\bar{\nu}\bar{\Omega}$ , because the kinematic viscosity depends also on the temperature  $T$ . To the contrary, if one invokes an assumption that  $\rho\nu = \rho_u\nu_u$ , which is typical for theoretical research into premixed flames and was used in DNS studies discussed in the end of Sec. III, then,  $\bar{\rho}\bar{\varepsilon} = 2\rho_u\nu_u\bar{\Omega}$ , i.e. the Favre-averaged dissipation rate is proportional to the Reynolds-averaged enstrophy. Accordingly, the Reynolds-averaged equation (9) will be considered in the rest of the paper.

### III. SIMULATIONS

Because DNS data analyzed here were discussed in detail in Refs. 28 and 36 and were already used in a number of recent papers,<sup>37–42</sup> we restrict ourselves to a brief summary of the simulations. The computational domain was a rectangular  $8 \times 4 \times 4$  mm and was resolved using a uniform rectangular mesh of  $512 \times 128 \times 128$  points. A statistically planar, 1D premixed flame was studied by solving unsteady 3D continuity, Navier-Stokes, and energy equations, as well as a balance equation for the mass fraction  $Y$  of the deficient reactant and the ideal gas state equation. Combustion chemistry was reduced to a single reaction, the Lewis and Prandtl numbers were equal to 1.0 and 0.75, respectively, and the dependence of the molecular transfer coefficients on the temperature  $T$  was taken into account, e.g.,  $\nu = \nu_u(T/T_u)^{1.7}$ . The combustion progress variable  $c = (T - T_u)/(T_b - T_u)$ .

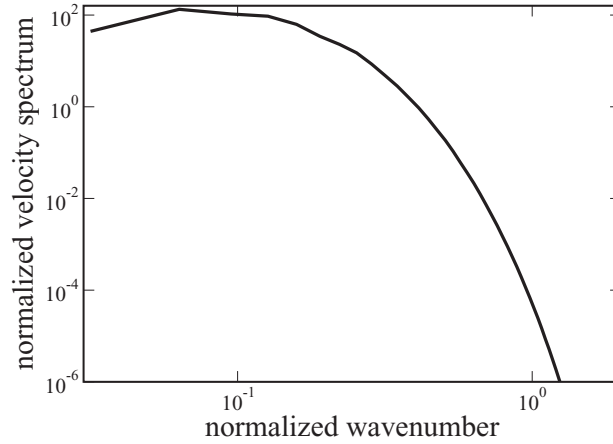


FIG. 1. Normalized velocity spectrum  $E(k)/(\bar{\epsilon}v_u^5)^{1/4}$  vs. normalized wavenumber  $kn$ .

Homogeneous isotropic turbulence ( $u' = 0.53$  m/s, integral length scale  $L = 3.5$  mm, Taylor microscale  $\lambda = 2.1$  mm, Kolmogorov scale  $\eta = 0.14$  mm, time scale  $\tau_t = L/u' = 6.6$  ms, and the turbulent Reynolds number  $Re_t = u'L/\nu_u = 96$ ) was pre-computed<sup>28</sup> in a cube with size of 4 mm and 256 grid points in each direction during about  $2\tau_t$ . The turbulence spectrum is shown in Fig. 1 and the aforementioned turbulence characteristics were evaluated as follows:

$$u' = \left( \frac{2}{3} \int_0^\infty E(k) dk \right)^{1/2}, \quad L = \frac{3\pi}{4} \frac{\int_0^\infty k^{-1} E(k) dk}{\int_0^\infty E(k) dk}, \quad (10)$$

$$\lambda = \left( \frac{10\nu_u}{\bar{\epsilon}} \int_0^\infty E(k) dk \right)^{1/2}, \quad \eta = \left( \frac{\nu_u^3}{\bar{\epsilon}} \right)^{1/4}, \quad \bar{\epsilon} = 2\nu_u \int_0^\infty k^2 E(k) dk.$$

The obtained statistically stationary turbulent field entered the computational domain with a mean velocity  $U$  through the inlet boundary  $x = 0$  and decayed along the direction  $x$  of the mean flow, e.g., see Fig. 2(a) in Sec. IV.

At  $t = 0$ , the pre-computed turbulent velocity field was assigned to the entire computational domain and a planar laminar flame was embedded into the flow field. Subsequently, the inflow velocity was increased at instants  $t_1$  and  $t_2$ , i.e.,  $U(0 \leq t < t_1) = S_L < U(t_1 \leq t < t_2) < U(t_2 \leq t) = S_t$ , in order to keep the flame in the computational domain till the end  $t_3$  of the simulations.

Results discussed in Sec. IV were solely obtained for  $t \geq t_2$ , with the instants  $t_2$  being different in three simulated cases. It is worth stressing that the mean inlet velocity was constant at  $t \geq t_2$ , with the inlet turbulence, mean flame position, speed, and brush thickness being statistically stationary. Averaging was performed both across the transverse  $yz$ -plane and over time interval  $t_2 \leq t \leq t_3$ , with  $t_3 - t_2 \approx 1.5\tau_t$ . Axial profiles  $\langle q|c \rangle(x)$  of various quantities  $q$  conditioned on a particular value  $c$  of the combustion progress variable were also obtained using a joint Probability Density Function (PDF)  $P(c, q, x)$ , which had been computed by processing the DNS data saved for a plane  $x = \text{const}$  at various instants  $t_2 \leq t \leq t_3$ . Subsequently, these profiles were transformed to  $\langle q|c \rangle(\bar{c})$  using the axial profiles  $\bar{c}(x)$  of the Reynolds-averaged combustion progress variable. Here, we use the Reynolds-averaged  $\bar{c}$ , because it is equal to the probability of finding combustion products under conditions of the present DNS.

Moreover, quantities  $\bar{q}_u = \langle q|c \leq \epsilon \rangle$  and  $\bar{q}_b = \langle q|1 - c \leq \epsilon \rangle$  conditioned on unburned and burned gas, respectively, were computed, as well as quantities  $\bar{q}_{f,u} = \langle q|\epsilon_1 \leq c \leq \epsilon_2 \rangle$  and  $\bar{q}_{f,b} = \langle q|\epsilon_1 \leq 1 - c \leq \epsilon_2 \rangle$  conditioned on unburned and burned edges of flame fronts, respectively. To assess the influence of  $\epsilon$ ,  $\epsilon_1$ , and  $\epsilon_2$ , we varied these parameters as follows;  $\epsilon = 0.02, 0.05, 0.1, 0.15$  and  $\{\epsilon_1, \epsilon_2\} = \{0.01, 0.02\}, \{0.01, 0.05\}, \{0.02, 0.05\}, \{0.02, 0.1\},$  and  $\{0.05, 0.1\}$ . Moreover, the following conditioned quantities  $\bar{q}_b = \bar{c}q/\bar{c}$  and  $\bar{q}_u = (1 - c)q/(1 - \bar{c})$  were also evaluated. Because similar results were obtained using all these constraints, we will restrict ourselves to reporting data computed for  $\epsilon = 0.02$  and  $\{\epsilon_1, \epsilon_2\} = \{0.01, 0.02\}$ .

TABLE I. Flame characteristics.

	Case H	Case M	Case L
$\rho_u/\rho_b$	7.53	5.0	2.5
$S_L$ , m/s	0.600	0.523	0.416
$\delta_L$ , mm	0.217	0.191	0.158
$Da_1$	18.3	18.1	17.4
$Da_2$	94	71	45
$Ka$	0.11	0.14	0.22
$S_t$ , m/s	1.13	1.0	0.74
$\delta_t$ , mm	1.23	1.41	1.35

Characteristics of three studied flames are reported in Table I, where  $\sigma = \rho_u/\rho_b$  is the density ratio,  $\delta_L = (T_b - T_u)/\max |dT/dx|$  is the laminar flame thickness,  $Da_k = \tau_t/\tau_{c,k}$  are the Damköhler numbers evaluated using two different chemical time scales, i.e.,  $\tau_{c,1} = \delta_L/S_L$  and  $\tau_{c,2} = \kappa_u/S_L^2$ , where  $\kappa_u$  is the heat diffusivity of unburned gas,  $Ka = Re_t^{1/2}/Da_2$  is the Karlovitz number, and  $\delta_t = 1/\max |d\bar{c}/dx|$  is the mean turbulent flame brush thickness.

It is worth noting that the simulations by Nishiki *et al.*<sup>28,36</sup> were run more than a decade ago. Since that, significant progress in the area of DNS of premixed turbulent combustion was made and the leading groups succeeded in directly computing highly turbulent flames by allowing for complex combustion chemistry.<sup>43–45</sup> When compared to the most advanced recent numerical simulations, the DNS analyzed by us is not state of the art. However, this fact does not mean that the data have no value today. Like the development of advanced laser diagnostic tools does not call for ignoring earlier experimental data obtained using “outdated” techniques, the rapid development of CFD soft- and hardware does not make earlier numerical data useless, especially as even an “outdated” DNS involves less simplifications than, e.g., a theoretical study or RANS computation. If a new approach to data processing is developed, it can be applied not only to recent, but also to earlier data. The novelty of the present work consists of a new analysis of well-known data.

Moreover, research into a problem requires tools that adequate to the research goals, while the use of more advanced, but more complicated and expensive tools does not seem to be the best solution always. For instance, implementation of complex combustion chemistry into a DNS software is of great value in order to investigate various important issues such as emissions, local quenching, and eventual re-ignition, etc. However, as far as the influence of combustion on vorticity and enstrophy fields is concerned, the effect is controlled by the local density variations, which can be modeled reasonably well within the framework of a single-step chemistry, unless the local quenching plays a substantial role. In particular, all previous target-directed DNS studies of vorticity transformation in premixed turbulent flames, which are further discussed in the end of this section, either dealt with a single-step chemistry,<sup>32–34</sup> or reduced combustion to self-propagation of an infinitely thin interface that separated unburned and burned gas.<sup>31</sup>

An increase in a ratio of  $u'/S_L$  addressed by a DNS is of great value in order to gain an insight into the physics of highly turbulent combustion, which is still poorly understood.<sup>3</sup> However, a range of  $u'/S_L = O(1)$  is of more interest for the goals of the present work, because the influence of combustion on vorticity field is more pronounced in weakly turbulent flames. Note, that the local quenching, which is sensitive to combustion chemistry, is unlikely to play a role in such weakly turbulent flames.<sup>3</sup>

An increase in feasible turbulent Reynolds number is another very important goal for researchers who develop advanced DNS tools. It is worth remembering, however, that the highest  $Re_t$  reached in DNS of premixed turbulent flames is significantly less than  $Re_t$  typical for contemporary DNS of non-reacting flows.<sup>46</sup> The point is that the scales of chemical reactions that control heat release are often much less than the Kolmogorov scales and the need for reducing the step of numerical mesh required to resolve those reactions impedes increasing a ratio of  $L/\eta \propto Re_t^{3/4}$ . Such a scale separation ( $\delta_L \ll \eta \ll L$ ) is particularly well pronounced in weakly turbulent flames associated with the strongest influence of combustion on turbulence. Accordingly, the range of  $Re_t \approx 100$  reached in

the DNS by Nishiki *et al.*<sup>28,36</sup> is typical even for recent simulations. For instance, among eight papers that aimed at DNS of premixed turbulent flames and were published in the proceedings of the latest 34th Combustion Symposium,<sup>45,47–53</sup>  $Re_t$  was substantially larger than 100 only in two papers,<sup>45,52</sup> with the combustion chemistry being reduced to a single reaction in five papers.<sup>47,49–51,53</sup> We may also note that the DNS data by Nishiki *et al.*<sup>28,36</sup> were analyzed in several recent papers.<sup>40–42</sup>

Nevertheless, the DNS by Nishiki *et al.*<sup>28,36</sup> suffered from a low ratio of the transverse width  $\Lambda_{yz} = 4$  mm of the computational domain to the integral length scale  $L = 3.5$  mm of turbulence. On the one hand, such a low ratio of  $\Lambda_{yz}/L$  is an obvious limitation. Nevertheless, as far as the goals of the present study are concerned, this limitation should not be overestimated, because (i) the governing phenomena, i.e., the baroclinic torque and dilatation, are localized to flame fronts, which are much thinner than the width  $\Lambda_{yz}$ , and (ii) small-scale effects are commonly less sensitive to the size of the computational domain. On the other hand, a low ratio of  $\Lambda_{yz}/L$  allowed Nishiki *et al.*<sup>28,36</sup> to reach sufficiently large ratios of  $L/\delta_L$ , whereas the vast majority of recent DNSs<sup>44,45,47–53</sup> are characterized by  $L/\delta_L = O(1)$ . A low ratio of  $L/\delta_L = O(1)$  is also an important limitation. If the instantaneous flame front is thin (when compared to  $\Lambda_{yz}$ ) and the primary physical mechanism of an increase in burning rate by turbulence consists of wrinkling the front by eddies larger than  $\delta_L$ , then, the range of eddies that can wrinkle a flame front in a DNS characterized by  $L/\delta_L = O(1)$  is much narrower than the range of eddies that can wrinkle a flame front in a typical laboratory experiment.<sup>3</sup> Unless 3D DNS of a premixed turbulent flame characterized by  $\delta_L < \eta \ll L \ll \Lambda_{yz}$  is routinely available, a researcher has to choose between two unpractical, but feasible cases, either  $\delta_L = O(L) \ll \Lambda_{yz}$  or  $\delta_L \ll L = O(\Lambda_{yz})$ . While the former case was selected in vast majority of recent DNS studies,<sup>44,45,47–53</sup> the latter case addressed, in particular, by Nishiki *et al.*<sup>28,36</sup> is also worth investigating.

To conclude this section, let us compare the present simulations with previous DNS research<sup>31–34</sup> into vorticity transformation in premixed turbulent flames.

Treurniet *et al.*<sup>31</sup> varied both  $u'/S_L = \{0.59, 1.17, 2.35\}$  and the density ratio  $\sigma = \{2, 4, 6\}$ . These researchers solved kinematic  $G$ -equation, thus, neglecting effects associated with a finite thickness of the instantaneous flame front, whereas the present simulations dealt with the balance equation for  $Y$  and allowed a finite thickness  $O(\delta_L)$  of the front. The product  $\rho v$  was constant in the study by Treurniet *et al.*<sup>31</sup>

Hamlington *et al.*<sup>32,33</sup> did not vary the density ratio  $\sigma = 7.3$  and addressed higher  $u'/S_L = 2.45 - 30.6$ , but low  $L/\delta_L = 1.9$ . Accordingly, the Damköhler number  $Da_1 = 0.78 - 0.06$  was lower than unity, while the Karlovitz number  $(2\delta_L/L)^{1/2}(u'/S_L)^{3/2} = 3.9 - 174$  was large, contrary to the DNS analyzed in the present paper. Moreover, Hamlington *et al.*<sup>32,33</sup> used forcing in order to obtain statistically stationary, homogeneous isotropic turbulence in unburned gas, whereas turbulence was statistically stationary, but decayed in the  $x$ –direction in the present work and in the simulations by Treurniet *et al.*<sup>31</sup> Furthermore,  $v = 0$  and small-scale eddies were dissipated due to numerical viscosity in the DNS by Hamlington *et al.*<sup>32,33</sup>

Chakraborty<sup>34</sup> analyzed two DNS databases. One dealt with a single weakly turbulent premixed flame with  $Le = 1$ ,  $\sigma = 3.3$ ,  $u'/S_L = 1.41$ ,  $L/\delta_L = 9.64$ ,  $Re_t = 56.7$ ,  $Da_2 = 6.84$ , and  $(\delta_L/L)^{1/2}(u'/S_L)^{3/2} = 0.54$ . Other attributes of that DNS were similar to the attributes of the DNS analyzed by us, but data were processed at a single instant and  $\rho v = \rho_u v_u$ . Another DNS database analyzed by Chakraborty<sup>34</sup> encompassed results computed for five flames characterized by various  $Le = \{0.34, 0.6, 0.8, 1.0, 1.2\}$  and  $\sigma = 5.5$  and one flame with  $Le = 1$  and  $\sigma = 4.0$ . In all six cases, turbulence decayed in time with the initial  $u'/S_L = 7.5$ ,  $L/\delta_L = 2.45$ ,  $Re_t = 47.0$ ,  $Da_2 = 0.33$ , and  $(\delta_L/L)^{1/2}(u'/S_L)^{3/2} = 13.2$ . The data were processed at a single instant and  $\rho v = \rho_u v_u$ . Because Chakraborty<sup>34</sup> placed the focus of his study on statistics of vorticity alignment with local strain rates, our results reported in Sec. IV cannot be compared straightforwardly with his findings.

#### IV. RESULTS AND DISCUSSION

Because 3D images of vorticity fields obtained in the present DNS were already reported by Nishiki *et al.*,<sup>28</sup> the focus of the following discussion is placed on quantitative characteristics of vorticity transformation in premixed turbulent flames.

### A. Mean and conditioned vorticity and enstrophy

Figure 2(a) shows variations in the mean magnitude  $\overline{\omega} = \overline{(\boldsymbol{\omega} \cdot \boldsymbol{\omega})}^{1/2}$  of vorticity vector along the axial distance  $x$ . In cases H and M characterized by a large and medium density ratio, respectively, flame can generate vorticity, but  $\overline{\omega}$  monotonously decreases with  $x$  in case L associated with a low  $\sigma$ . Similar trends were obtained by Treurniet *et al.*<sup>31</sup> for  $\sigma = 2, 4$ , and 6, whereas Hamlington *et al.*<sup>32</sup> reported a decrease in the magnitude of vorticity within flame brush in the case of  $\sigma = 7.3$ , with the effect being less pronounced at larger  $u'/S_L$ . However, straightforward comparison of the present results with the results computed by Hamlington *et al.*<sup>32</sup> is difficult, because the two studies addressed turbulent flames associated with different combustion regimes ( $Da \gg 1$  and  $Ka \ll 1$  in the present work, but  $Da < 1$  and  $Ka > 1$  in the cited paper) and different turbulence length scales ( $L \gg \delta_L$  and  $L = O(\delta_L)$ , respectively).

As already found in earlier studies,<sup>31,32</sup> a flame makes vorticity field substantially anisotropic. For instance, Fig. 2(b) shows that flames H and M increase the Favre rms vorticity components  $[\rho(\omega_i - \bar{\omega}_i)^2/\bar{\rho}]^{1/2}$  in the tangential  $y$  and  $z$  directions at  $\bar{c} > 0.5$ , see dashed curves 2 and dotted-dashed curves 3, respectively, whereas the normal component  $\omega'_x$  decreases monotonously with  $x$  (solid curves 1). It is worth noting that the mean values  $\bar{\omega}_i$  are much less than  $\omega'_i$  for all ( $i = 1, 2, 3$ ) components of the vorticity vector and, therefore,  $(\omega_i - \bar{\omega}_i)^2 \approx \omega_i^2$  and  $\overline{\Omega^2} \approx \overline{\boldsymbol{\omega} \cdot \boldsymbol{\omega}}/2$  under conditions of the present DNS. As far as difference in the magnitudes of the peak values of  $\overline{(\boldsymbol{\omega} \cdot \boldsymbol{\omega})}^{1/2}$ , see Fig. 2(a), and  $[\rho(\omega_k - \bar{\omega}_k)(\omega_k - \bar{\omega}_k)/\bar{\rho}]^{1/2}$ , see curves 4 in Fig. 2(b), is concerned, it results from the difference in averaging methods, i.e., Reynolds and Favre ones, respectively.

Figure 3 shows that, in cases H and M, (i) the magnitude of the vector  $\boldsymbol{\omega}$  that is conditioned on burned mixture or burned edge of flamelets (i.e., instantaneous thin, inherently laminar flame fronts) is increased with  $\bar{c}$ , (ii)  $\bar{\omega}_{f,u}$  is almost constant (H) or weakly decreased (M), while (iii)  $\bar{\omega}_u$  is decreased with  $\bar{c}$ . In case L, all the conditioned vorticities are decreased, with the effect being least pronounced for  $\bar{\omega}_{f,b}$ .

Figure 4(a) indicates that enstrophy is generated in the middle of flamelets in case H and a similar trend is observed in case M (not shown). In case L, the effect is weakly pronounced only at large  $\bar{c}$ , see dotted-dashed curve in Fig. 4(b), whereas  $\langle \Omega | c \rangle$  decreases with  $c$  at  $\bar{c} \leq 0.5$ .

In all cases, the behavior of conditioned magnitude  $\langle \omega_t | c \rangle$  of the locally tangential (to flamelets) component  $\boldsymbol{\omega}_t = \boldsymbol{\omega} - \mathbf{n}(\boldsymbol{\omega} \cdot \mathbf{n})$  of the vorticity vector is similar to the behavior of  $\langle 2\Omega | c \rangle$ , cf. curves in Figs. 4(a) and 4(b) with the counterpart curves shown in bold lines in Figs. 5(a) and 5(b), respectively. Here,  $\mathbf{n} = -\nabla c / |\nabla c|$  is the unit vector normal to a flamelet and the magnitude  $\omega_t$  is equal to  $(\boldsymbol{\omega}_t \cdot \boldsymbol{\omega}_t)^{1/2}$ . The conditioned magnitude  $\langle \omega_n | c \rangle$  of the locally normal component  $\boldsymbol{\omega}_n = \mathbf{n}(\boldsymbol{\omega} \cdot \mathbf{n})$  decays within flamelets in all cases, see thin lines in Figs. 5(a) and 5(b). Here,  $\omega_n = (\boldsymbol{\omega}_n \cdot \boldsymbol{\omega}_n)^{1/2}$ .

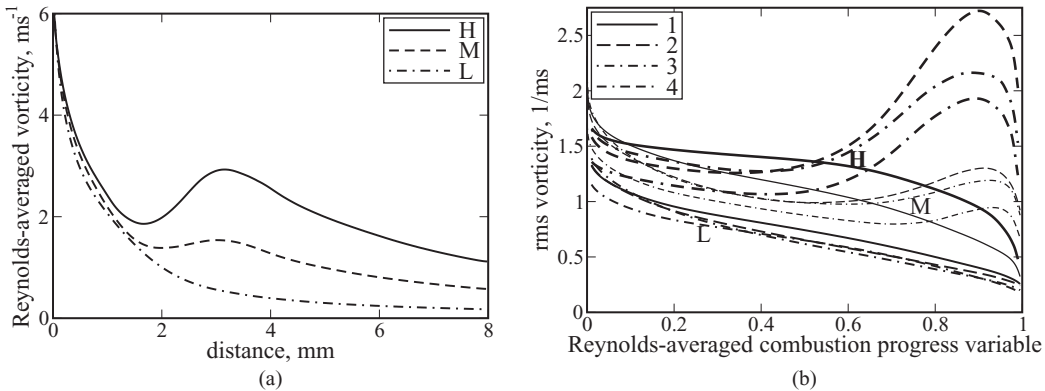


FIG. 2. (a) Dependence of the Reynolds averaged magnitude  $\overline{(\boldsymbol{\omega} \cdot \boldsymbol{\omega})}^{1/2}$  of vorticity vector  $\boldsymbol{\omega}$  on the axial distance  $x$ . (b) Variations in the Favre rms vorticity components  $\omega'_i \equiv [\rho(\omega_i - \bar{\omega}_i)^2/\bar{\rho}]^{1/2}$  within flame brush. 1 -  $[\rho(\omega_x - \bar{\omega}_x)^2/\bar{\rho}]^{1/2}$ , 2 -  $[\rho(\omega_y - \bar{\omega}_y)^2/\bar{\rho}]^{1/2}$ , 3 -  $[\rho(\omega_z - \bar{\omega}_z)^2/\bar{\rho}]^{1/2}$ , 4 - the sum  $[\rho(\omega_k - \bar{\omega}_k)(\omega_k - \bar{\omega}_k)/\bar{\rho}]^{1/2}$  of 1, 2, and 3.

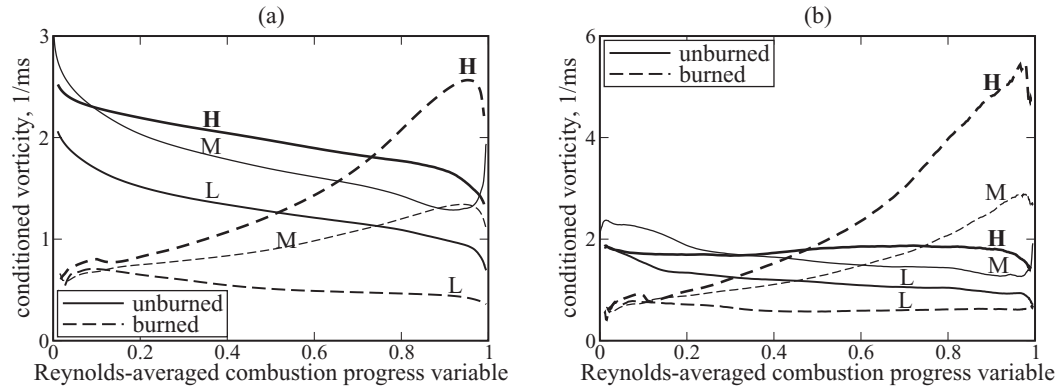


FIG. 3. Variations in the magnitude of vorticity vector conditioned on (a) unburned or burned gas and (b) unburned or burned edges of flamelets within flame brush.

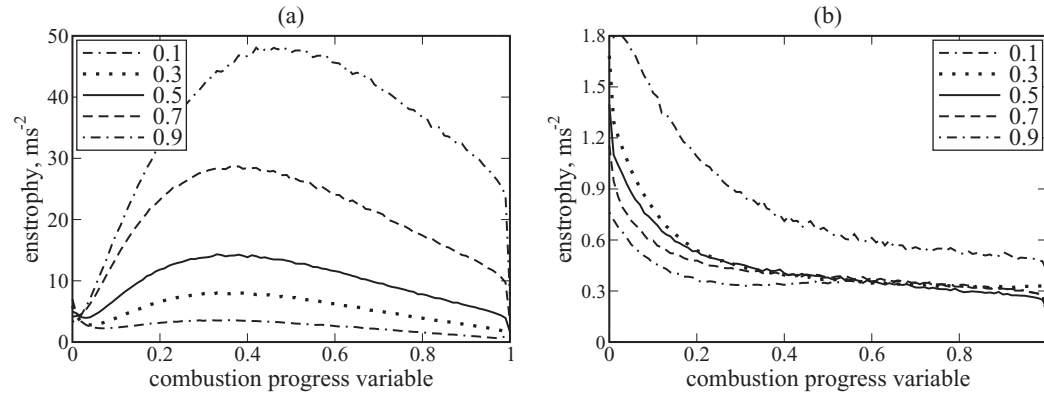


FIG. 4. Dependencies of conditioned enstrophy ( $2|\Omega|c$ ) on  $c$ , obtained at various Reynolds-averaged  $\bar{c}$  specified in legends in cases (a) H and (b) L.

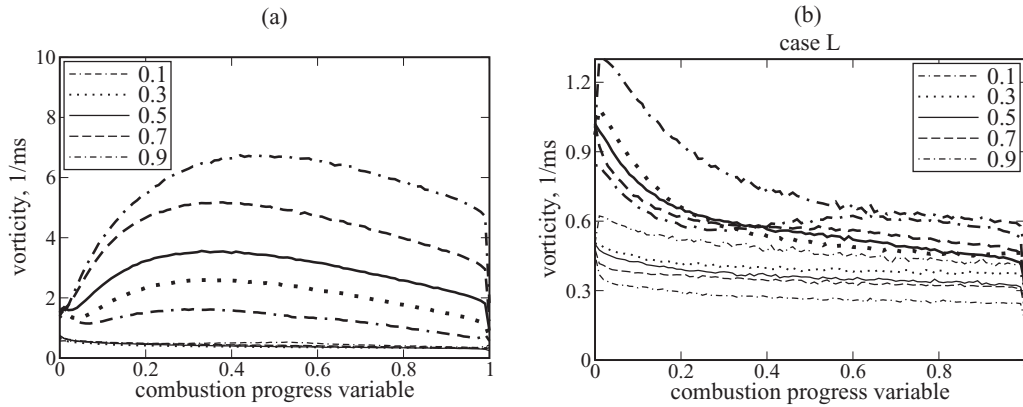


FIG. 5. Dependencies of conditioned magnitudes of the locally tangential (bold lines) and normal (thin lines) components of the vorticity vector on  $c$ , obtained at various Reynolds-averaged  $\bar{c}$  specified in legends in cases (a) H and (b) L.

## B. Conditioned and mean terms in vorticity and enstrophy balance equations

At a first glance, the generation of locally tangential vorticity in flames H and M could be attributed to the baroclinic torque term in Eq. (2). Indeed, Fig. 6 shows that the conditioned magnitude  $\langle T_{4t}|c \rangle$  of locally tangential component  $\mathbf{T}_{4t} = \mathbf{T}_4 - \mathbf{n}(\mathbf{T}_4 \cdot \mathbf{n})$  of the baroclinic torque vector  $\mathbf{T}_4 = \rho^{-2} \nabla \rho \times \nabla p$ , see thin lines, is larger than the conditioned magnitude  $\langle T_{3t}|c \rangle$  of locally tangential component of the dilatation vector-term  $\mathbf{T}_3 = \boldsymbol{\omega}(\nabla \cdot \mathbf{u})$ , see bold lines, everywhere in flamelets in

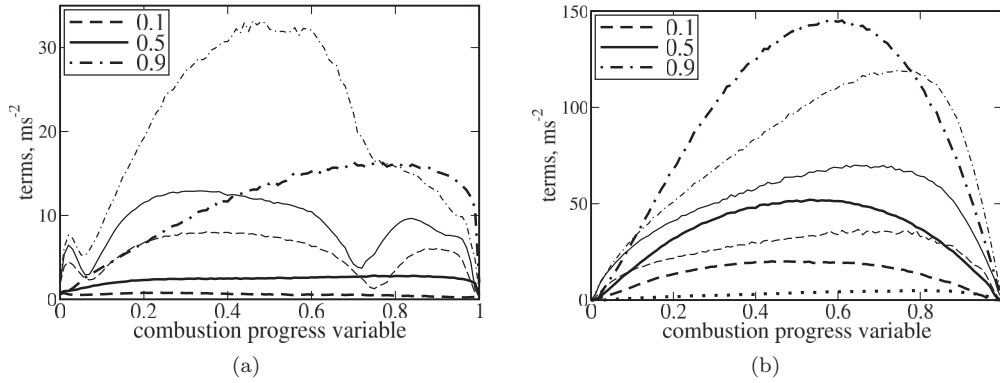


FIG. 6. Dependencies of conditioned magnitudes  $\langle(\mathbf{T}_t \cdot \mathbf{T}_t)^{1/2}|c\rangle$  of locally tangential components  $\mathbf{T}_t = \mathbf{T} - \mathbf{n}(\mathbf{T} \cdot \mathbf{n})$  of vector terms  $\mathbf{T}$  in the vorticity Eq. (2), on  $c$ , obtained at various  $\bar{c}$  specified in legends. (a) Bold and thin lines show the vortex-stretching  $\mathbf{T}_1 = (\boldsymbol{\omega} \cdot \nabla)\mathbf{u}$  and viscous  $\mathbf{T}_2$  terms, respectively, in case H. (b) Bold and thin lines show the dilatation  $\mathbf{T}_3 = \boldsymbol{\omega}(\nabla \cdot \mathbf{u})$  and baroclinic torque  $\mathbf{T}_4 = \rho^{-2}\nabla\rho \times \nabla p$  terms, respectively, in case H. Dotted curve shows the baroclinic torque term at  $\bar{c} = 0.9$  in case L.

case H if  $\bar{c} = 0.1$  or  $0.5$ . The magnitudes of two other conditioned terms  $\langle T_{1t}|c\rangle$  and  $\langle T_{2t}|c\rangle$  are much lower, cf. Figs. 6(a) and 6(b).

Thus, anisotropic generation of vorticity in cases H and M is associated with the baroclinic torque to the leading order, whereas the conditioned vorticity  $\bar{\omega}_u$  is decreased with  $\bar{c}$ , see solid curves in Fig. 3(a), because the baroclinic torque vanishes in the unburned gas. Because small angles between  $\nabla\rho$  and the  $x$ -axis are statistically more significant, the baroclinic torque affects  $\omega_x$  weaker than  $\omega_y$  or  $\omega_z$ , cf. curves 1 with curves 2 and 3 in Fig. 2(b), whereas the dilatation term efficiently reduces all the three components of  $\boldsymbol{\omega}$ . Similarly, the conditioned magnitude  $\langle(\boldsymbol{\omega}_t \cdot \boldsymbol{\omega}_t)^{1/2}|c\rangle$  of the locally tangential component of the vorticity vector is increased by the baroclinic torque, whereas the locally normal component is damped due to the dilatation. The aforementioned trends are less pronounced in flame M, because the baroclinic torque term is decreased when the density ratio is reduced. For instance, in an unperturbed laminar flame,  $\rho^{-2}|\nabla\rho| = |\nabla\mathbf{u}|/(\rho_u S_L) \propto (\sigma - 1)/(\rho_u \delta_L)$  and  $|\nabla p| \propto (\sigma - 1)\rho_u S_L^2/\delta_L$ .

In flame L, the vorticity field remains sufficiently isotropic and decays, because the influence of the flame on the field is weak due to a low magnitude of the baroclinic torque term in Eq. (2), cf. dotted and thin dotted-dashed lines in Fig. 6(b). Note that  $(\sigma - 1)^2$  is larger by a factor of about 20 in case H when compared to case L.

The following trends indicated in Fig. 6(b) are also worth noting. First, the shape of  $\langle T_{4t}|c\rangle(c)$ -curves is mainly controlled by the dependence of  $\rho^{-2}|\nabla\rho|$  on  $c$  in the counterpart laminar flame (not shown), while the dependence of the magnitude  $|(\nabla p)_t|$  of the locally tangential pressure gradient on  $c$  is weakly pronounced, see Fig. 7(a), because  $(\nabla p)_t$  is mainly controlled by the heat release in surrounding flamelets. To the contrary, the magnitude  $|\nabla p|$  of the complete pressure gradient in flamelets is substantially affected by the local heat release and depends strongly on  $c$ , see Fig. 7(b), but these effects are relevant to the normal component  $\nabla p \cdot \mathbf{n}$ , which does not contribute to the baroclinic torque. The shape of  $\langle T_{3t}|c\rangle(c)$ -curves is also controlled by the dependence of  $\rho^{-2}|\nabla\rho|$  on  $c$  due to the continuity equation ( $\nabla \cdot \mathbf{u} = -\mathbf{u} \cdot \nabla\rho/\rho = \rho_u S_L |\nabla\rho|/\rho^2$  in the unperturbed laminar premixed flame).

Second, an increase in  $\langle T_{4t}|c\rangle$  with the Reynolds-averaged  $\bar{c}$ , cf. dashed, solid, and dotted-dashed thin lines in Fig. 6(b), is associated with an increase in  $|(\nabla p)_t|$  with  $\bar{c}$ , see Fig. 7(a). Because the pressure gradient produced by surrounding flamelets is statistically parallel to the  $x$ -axis, which is normal to the mean flame brush, the locally tangential component  $|(\nabla p)_t|$  is larger when an angle between the flamelet surface and the  $x$ -axis is lower. Indeed, Fig. 8(a) indicates that conditioned  $\langle n_x|c\rangle$  is lower for larger  $\bar{c}$ , i.e., the probability of finding flamelets that are locally normal to the mean flame brush is higher at its trailing edge.

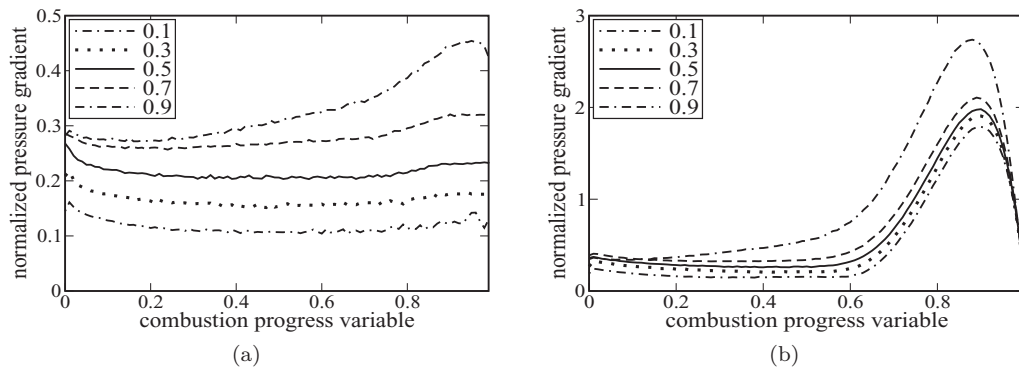


FIG. 7. Dependencies of normalized conditioned magnitudes of (a) tangential and (b) complete pressure gradients on  $c$ , obtained in case H at various Reynolds-averaged  $\bar{c}$  specified in legends. Normalization was done using  $\rho_u S_L \max |du/dx|$  evaluated in the laminar flame H.

Third, the increase in  $\langle T_{4t}|c \rangle$  with  $\bar{c}$  results in increasing enstrophy, see Fig. 4(a). Therefore, the dilatation term is also increased, see bold lines in Fig. 6(b), because its magnitude is proportional to  $|\omega|$ .

However, highlighting solely the baroclinic torque oversimplifies the problem. This physical mechanism can not only generate, but also damp vorticity, depending on an angle between the vorticity and baroclinic torque vectors. At the leading edge of a flamelet, directions of  $\omega$  and  $\nabla\rho \times \nabla p$  appear to be statistically independent, see Fig. 8(b), and the baroclinic torque term plays a minor role in the enstrophy Eq. (8), at low  $c$ , because an increase and a decrease in  $\omega$  statistically balance one another. Deeper in the flamelet, the two directions begin to correlate due to locally generated vorticity that is co-directed with the baroclinic torque vector. This effect is more pronounced at larger Reynolds-averaged  $\bar{c}$ , because the magnitude of the baroclinic torque vector is increased with  $\bar{c}$ , as discussed above. Nevertheless, even at large  $c$  and large  $\bar{c}$ , directions of the vectors  $\omega$  and  $\nabla\rho \times \nabla p$  are statistically different, see Fig. 8(b). Therefore, relative magnitude of the baroclinic torque with respect to the dilatation is lower in the enstrophy Eq. (8), when compared to the vorticity Eq. (2).

Accordingly, the budget of conditioned terms in the vorticity Eq. (2), see Fig. 6, differs substantially from the budget of various conditioned terms  $\langle T_k|c \rangle$  in the enstrophy Eq. (8). The conditioned enstrophy budget for  $\bar{c} = 0.5$  in case H is reported in Fig. 9(a) and similar results were obtained

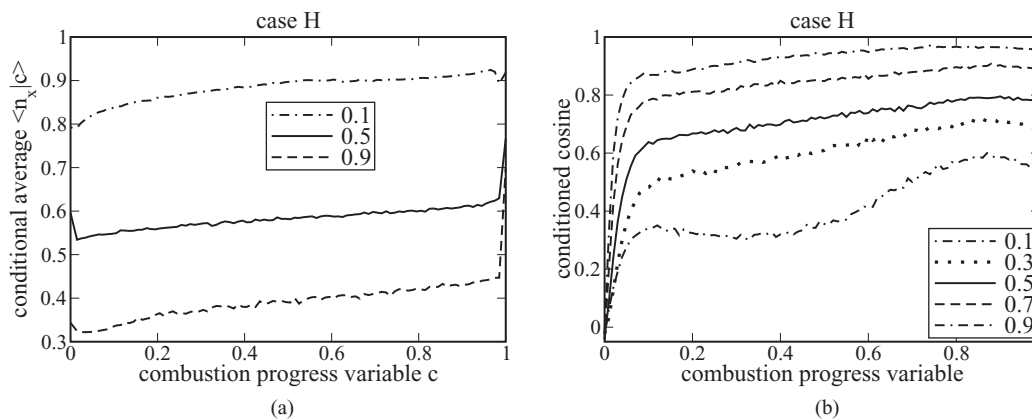


FIG. 8. Dependencies of conditioned (a)  $x$ -component  $\langle n_x|c \rangle$  of the unit normal vector  $\mathbf{n} = -\nabla c/|\nabla c|$  and (b) cosine  $\langle \omega \cdot (\nabla\rho \times \nabla p)/(|\omega| \cdot |\nabla\rho \times \nabla p|)|c \rangle$  of an angle between vorticity and baroclinic torque vectors on the combustion progress variable  $c$ , obtained at various Reynolds-averaged  $\bar{c}$  specified in legends. The component  $n_x$  is normal to the mean flame brush.

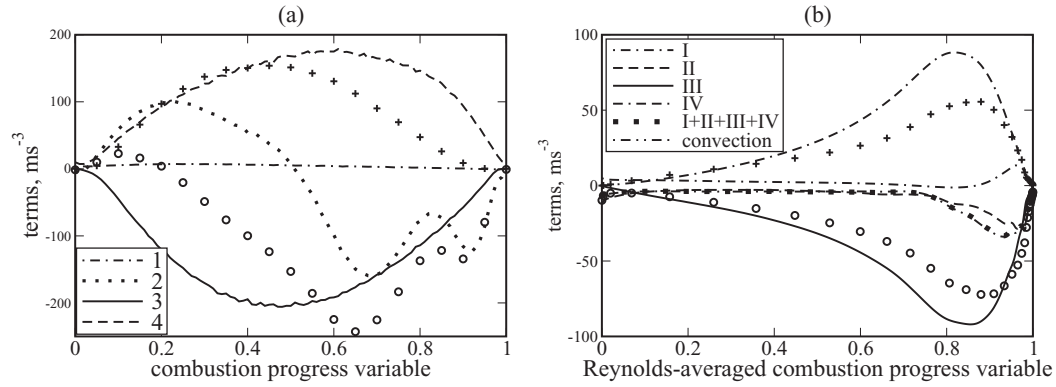


FIG. 9. Enstrophy balance in case H. Pluses and circles show subterms  $T_{21}$  and  $T_{22}$ , respectively. (a) Conditionally averaged terms  $\langle T_k | c \rangle$  in Eq. (8) vs.  $c$  at the Reynolds-averaged  $\bar{c} = 0.5$ . (b) Mean terms  $\bar{T}_k$  in Eq. (9) vs.  $\bar{c}$ .

in case M and for other  $\bar{c}$ , with the magnitude of terms 2–4 being increased by  $\bar{c}$ . In cases H and M (not shown), (i) the dilatation term 3 statistically overwhelms the baroclinic torque term 4 in the largest part of flamelets ( $c < 0.7$ ) and (ii) the viscous term  $\langle T_2 | c \rangle = \langle T_{21} + T_{22} | c \rangle$  (curve 2) plays an important role by redistributing  $\Omega$  inside flamelets (increasing/decreasing the enstrophy at lower/larger  $c$ ). Therefore, an increase in  $\langle \Omega | c \rangle$  with  $c$  at  $c < 0.4$ , see Fig. 4(a), is controlled not only by the local baroclinic torque term  $\langle T_4 | c \rangle$ , but also by the local viscous term  $\langle T_2 | c \rangle$  or, more precisely, by the contribution  $\langle T_{21} | c \rangle$  (pluses) of density variations to the viscous term. In particular, this term controls an increase in  $\langle \Omega | c \rangle$  at  $\bar{c} = 0.9$ , see dotted-dashed curve in Fig. 4(a), despite  $\langle T_4 | c \rangle$  is lower than  $\langle T_3 | c \rangle$  at  $c < 0.8$ , cf. thin and bold dotted-dashed lines in Fig. 6(b). To the best of the present authors knowledge, such a role of the viscous term has not yet been pointed out in the literature. In the DNS by Treurniet *et al.*,<sup>31</sup> flamelet structure was not resolved, while viscous effects were not addressed in the DNS study by Hamlington *et al.*<sup>32</sup>

Averaging of  $\langle T_2 | c \rangle$  over  $c$  reduces its magnitude significantly, cf. curves 2 in Figs. 9(a) and 9(b), because the mean subterms  $\bar{T}_{21}$  and  $\bar{T}_{22}$  counterbalance one another.<sup>54</sup> Accordingly, the viscous term II plays a minor role in the balance equation (9) for the mean enstrophy, with exception of the trailing edge of the flame brush, see curve II in Fig. 9(b). At any  $\bar{c}$ , the viscous term II is negative, thus, reducing the mean  $\bar{\Omega}$ .

Under conditions of the present DNS, the stretching term I in Eq. (9) is small, see curve I in Fig. 9(b). It is worth noting, however, that it is increased with  $u'$  and can dominate in highly turbulent flames.<sup>32</sup>

In case H, the dilatation term III and the baroclinic torque term IV dominate on the RHS of Eq. (9) and counterbalance one another, see Fig. 9(b), with the magnitude of the former term being slightly larger. Therefore, the sum of terms I–IV is negative (dotted curve). Note that this curve is very close to dashed-double-dotted curve, which shows the LHS of Eq. (9), thus, validating the present results.

The relations  $|\bar{T}_{III}| \approx |\bar{T}_{IV}|$  with  $|\bar{T}_{III}| > |\bar{T}_{IV}|$ , obtained in case H associated with substantial vorticity generation, could be explained as follows. If the baroclinic torque term 4 in Eq. (2) is large, this mechanism produces vorticity  $\omega_b$  in the direction of the vector  $\mathbf{b} = \nabla \rho \times \nabla p$ . The increase in  $\omega_b$  results in increasing the dilatation term 3 until its  $b$ -component counterbalances term 4 (if other terms are much less). However, in the enstrophy Eq. (8), the dilatation term 3 and the baroclinic torque term 4 involve  $|\omega| \geq \omega_b$  and  $\cos(\mathbf{b} \cdot \widehat{\omega}) \leq 1$ , respectively. Consequently, term III is slightly larger than term IV in this limit case.

It is worth noting that the mean baroclinic torque term  $\bar{T}_{IV}$  in Eq. (9) peaks at  $\bar{c} \approx 0.8$ , see dotted-dashed curve IV in Fig. 9(b), whereas Fig. 6(b), cf. thin solid and dotted-dashed lines, Fig. 7(a), see double-dashed-dotted curve, and Fig. 8(a), see dashed curve, imply that the conditioned baroclinic torque term in Eq. (8) is still increased by  $\bar{c}$  even if  $\bar{c} > 0.8$ . The point is that the dependence of the mean term  $\bar{T}_{IV}$  on the mean combustion progress variable is controlled not only

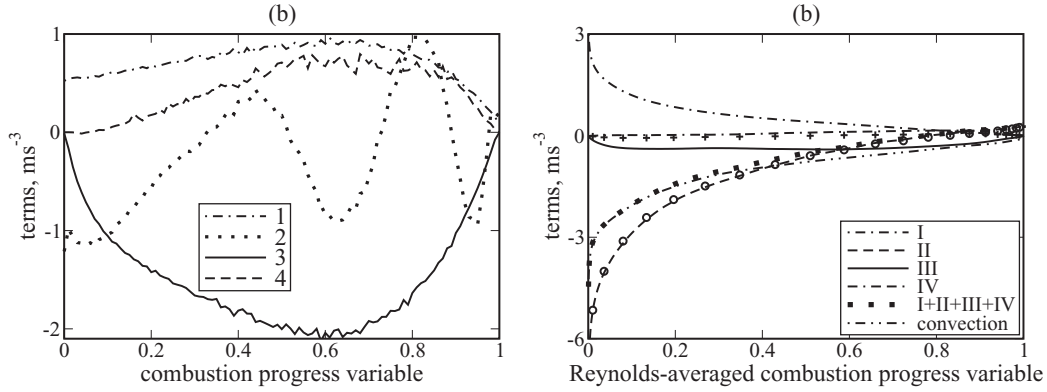


FIG. 10. Enstrophy balance in case L. Pluses and circles show subterms  $T_{21}$  and  $T_{22}$ , respectively. (a) Conditionally averaged terms  $\langle T_k | c \rangle$  in Eq. (8) vs.  $c$  at the Reynolds-averaged  $\bar{c} = 0.5$ . (b) Mean terms  $\overline{T}_k$  in Eq. (9) vs.  $\bar{c}$ .

by the dependence of the magnitude  $\langle (\mathbf{T}_4 \cdot \mathbf{T}_4)^{1/2} | c \rangle$  of the conditioned term on the mean  $\bar{c}$ , but also by the probability of finding flamelets, which peaks typically at lower  $\bar{c} \approx 0.5$ .

In case L, the dilatation dominates in flamelets and damps enstrophy jointly with the viscous term 2, see Fig. 10(a). Comparison of Figs. 9(a) and 10(a) shows that the decrease in the density ratio strongly (by a factor of about 100) reduces the dilatation term, cf. solid curves, whereas a decrease in  $\sigma$  from 7.53 to 2.5 reduces the dilatation term in the counterpart laminar flames only by a factor of about five if  $\nabla \cdot \mathbf{u} \propto (\sigma - 1)S_L/\delta_L$ . The point is that (i) the conditioned dilatation term  $\langle T_3 | c \rangle$  in Eq. (8) is proportional not only to  $\nabla \cdot \mathbf{u}$ , but also to the conditioned enstrophy and (ii)  $\langle \Omega | c \rangle$  computed at  $\bar{c} = 0.5$  in case H is larger by a factor of about 30 when compared to case L, cf. solid lines in Figs. 4(a) and 4(b), respectively.

Moreover, the decrease in the density ratio reduces the conditioned baroclinic torque term  $\langle T_4 | c \rangle$ , cf. dashed curves in Figs. 9(a) and 10(a), even stronger when compared with the conditioned dilatation term  $\langle T_3 | c \rangle$ , cf. solid curves. The point is that the decrease in the density ratio not only similarly reduces  $|\nabla \rho|/\rho^2$  and  $\nabla \cdot \mathbf{u}$ , which is equal to  $\rho_u S_L |\nabla \rho|/\rho^2$  in the unperturbed laminar premixed flame, but also reduces the tangential pressure gradient in  $\langle T_4 | c \rangle$ .

Even if the dilatation dominates in flamelets in case L, see Fig. 10(a), flamelet contribution to the balance of the mean enstrophy is small due to a low probability of finding flamelets. Accordingly, the viscous term II dominates in Eq. (9) reducing  $\overline{\Omega}$ , see Fig. 10(b). Therefore, the decrease in the mean and conditioned enstrophies, reported in case L in Fig. 2(a), see dotted-dashed curve, and Fig. 3(a), respectively, is controlled by the viscous dissipation to the leading order.

### C. Dilatation fluctuations

At a first glance, results reported in Figs. 2(a) and 9(b) contradict one another, i.e.,  $|\overline{\omega}|$  is increased in the middle ( $0.4 < \bar{c} < 0.9$  if the  $x$ -dependence plotted in Fig. 2(a) is transformed to the  $\bar{c}$ -dependence) of H-flame brush despite the negative sign of the LHS and RHS of Eq. (9). This ‘‘paradox’’ is explained in Fig. 11(a), which shows that the convection term 2 on the RHS of the following equation

$$\underbrace{\overline{\mathbf{u} \cdot \nabla \Omega}}_1 = \underbrace{\overline{\mathbf{u} \cdot \nabla \Omega}}_2 + \underbrace{\overline{\mathbf{u}' \cdot \nabla \Omega'}}_3 \quad (11)$$

is positive in the middle of the flame brush despite the negative sign of the LHS. Figure 11(a) indicates an important role played by a correlation  $\overline{\mathbf{u}' \cdot \nabla \Omega'}$ . Similar results were obtained in case M (not shown), whereas term 3 was much lower than terms 1 and 2 in Eq. (11) in case L. In some sense, the correlation  $\overline{\mathbf{u}' \cdot \nabla \Omega'}$  controls an increase in the mean enstrophy in the H-flame brush, i.e., even if  $|\overline{T_{III}}|$  and  $|\overline{T_{IV}}|$  are much larger than  $|\overline{\mathbf{u}' \cdot \nabla \Omega'}|$ , the magnitude of the difference  $|\overline{T_{IV}} - \overline{T_{III}}|$  is

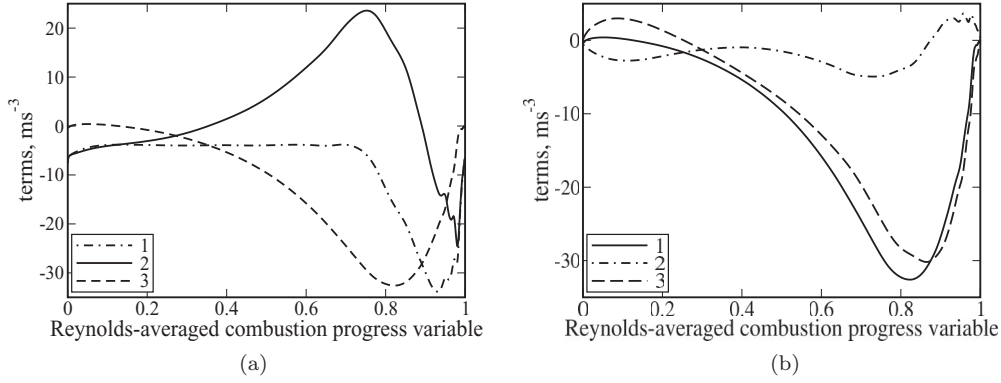


FIG. 11. Various terms in (a) Eq. (11) and (b) Eq. (12) in case H. Term numbers are specified in legends.

lower. To the best of our knowledge, such an important role played by the correlation has not yet been discussed.

The correlation is negative due to viscous decay of turbulence and intermittency of unburned and burned mixtures. If the combustion products arrive at a point  $\mathbf{x}$  within the flame brush, the  $x$ -component of the flow velocity is statistically increased due to the density drop and the rate of the viscous decay of the enstrophy is statistically increased due to an increase in the viscosity, with  $u_x$  and  $\partial\Omega/\partial x$  being predominately positive and negative, respectively. Therefore, such events are associated with predominately negative  $u'_x(\partial\Omega/\partial x)'$ . Similarly, when the unburned gas arrives at the same point,  $u'_x < 0$ , while  $(\partial\Omega/\partial x)' > 0$  (lower magnitude of negative  $\partial\Omega/\partial x$  when compared to its mean value), and, hence,  $u'_x(\partial\Omega/\partial x)'$  is predominately negative again. As far as term 1 on the LHS of Eq. (11) is concerned, it is negative because  $u_x$  and  $\partial\Omega/\partial x$  are predominately positive and negative, respectively. DNS data (not shown) indicate that the flamelet contribution to the term 1 is also negative, but the product contribution dominates at large  $\bar{c}$  associated with the peak magnitude of the term 1.

The correlation  $\overline{\mathbf{u}' \cdot \nabla \Omega'}$  can be rewritten as follows

$$\overline{\mathbf{u}' \cdot \nabla \Omega'} = \underbrace{\nabla \cdot \overline{\Omega' \mathbf{u}'}}_2 - \underbrace{\overline{\Omega' (\nabla \cdot \mathbf{u}')}}_3 \quad (12)$$

and, consequently, Eq. (9) reads

$$\begin{aligned} & \bar{u}_k \frac{\partial \bar{\Omega}}{\partial x_k} + \frac{\partial}{\partial x_k} \left( \overline{u'_k \Omega'} \right) \quad (13) \\ & = \underbrace{\overline{\omega_i \omega_k \frac{\partial u_i}{\partial x_k}}}_I + \underbrace{\varepsilon_{ijk} \omega_i \frac{\partial}{\partial x_j} \left( \frac{1}{\rho} \frac{\partial \tau_{kl}}{\partial x_l} \right)}_{II} - \underbrace{2\bar{\Omega} \frac{\partial u_k}{\partial x_k}}_{III} + \underbrace{\varepsilon_{ijk} \frac{1}{\rho^2} \omega_i \frac{\partial \rho}{\partial x_j} \frac{\partial p}{\partial x_k}}_{IV} + \underbrace{\overline{\Omega' \frac{\partial u'_k}{\partial x_k}}}_V. \end{aligned}$$

Figure 11(b) shows that (i) the magnitude of term 2 on the RHS of Eq. (12), see dotted-dashed curve, is significantly smaller than the magnitude of terms 1 and 3, see solid and dashed curves, respectively. Therefore, the correlation  $\overline{\mathbf{u}' \cdot \nabla \Omega'}$  is mainly controlled by the correlation  $\overline{\Omega' (\nabla \cdot \mathbf{u}')}$  between fluctuations in the enstrophy and dilatation. As Fig. 11(b) shows  $-\overline{\Omega' (\nabla \cdot \mathbf{u}')}$ , the correlation is positive. Accordingly, it is a source term on the RHS of Eq. (13), see term V, i.e., dilatation fluctuations reduce the damping effect of the mean dilatation term III. The correlation  $\overline{\Omega' (\nabla \cdot \mathbf{u}')}$  is positive, because high instantaneous positive values of both enstrophy and dilatation are localized to flamelets.

## V. CONCLUSIONS

Vorticity transformation in three weakly turbulent premixed flames characterized by three different density ratios  $\sigma$  was studied by processing a well-known DNS database and anisotropic

generation of vorticity within the flame brush was observed in cases H and M characterized by  $\sigma = 7.53$  and 5.0, respectively.

Various terms in vorticity and enstrophy balance equations, either mean or conditioned on a particular value  $c$  of the combustion progress variable, were analyzed. Besides widely recognized role played by baroclinic torque in vorticity generation, the following findings are worth emphasizing.

First, when the mean combustion progress variable is increased, the mean angle between the normals to flamelet and mean flame brush is also increased, thus, increasing pressure gradient tangential to flamelets and, hence, the magnitude of the baroclinic torque term in the vorticity balance equation. As a result, the magnitude of baroclinic torque term conditioned on flamelets is high at large  $\bar{c}$ .

Second, viscous effects substantially redistribute enstrophy within flamelets due to density variations, but play a minor role in the balance of the mean enstrophy  $\bar{\Omega}$  within turbulent flame in cases H and M and control the dissipation of  $\bar{\Omega}$  in case L ( $\sigma = 2.5$ ).

Third, negative correlation  $\overline{\mathbf{u}' \cdot \nabla \Omega'}$  between fluctuations in velocity and enstrophy gradient contributes substantially to an increase in the mean  $\bar{\Omega}$  within turbulent flame brush in cases H and M. As this important negative correlation is mainly controlled by the positive correlation between fluctuations in the enstrophy and dilatation, dilatation fluctuations substantially reduce the damping effect of the mean dilatation on the vorticity and enstrophy fields.

## ACKNOWLEDGMENTS

The work was supported by the Chalmers e-Science Centre, Combustion Engine Research Center (CERC), and Swedish Energy Agency.

- <sup>1</sup> R. W. Bilger, S. B. Pope, K. N. C. Bray, and J. F. Driscoll, "Paradigms in turbulent combustion research," *Proc. Combust. Inst.* **30**, 21 (2005).
- <sup>2</sup> T. Poinso and D. Veynante, *Theoretical and Numerical Combustion*, 2nd ed. (Edwards, Philadelphia, 2005).
- <sup>3</sup> A. Lipatnikov, *Fundamentals of Premixed Turbulent Combustion* (CRC Press, Boca Raton, Florida, 2012).
- <sup>4</sup> L. D. Landau and E. M. Lifshitz, *Fluid Mechanics* (Pergamon Press, Oxford, UK, 1987).
- <sup>5</sup> B. Karlovitz, D. W. Denniston, and F. E. Wells, "Investigation of turbulent flames," *J. Chem. Phys.* **19**, 541 (1951).
- <sup>6</sup> A. N. Lipatnikov and J. Chomiak, "Effects of premixed flames on turbulence and turbulent scalar transport," *Prog. Energy Combust. Sci.* **36**, 1 (2010).
- <sup>7</sup> T. Poinso, D. Veynante, and S. Candel, "Quenching processes and premixed turbulent combustion diagrams," *J. Fluid Mech.* **228**, 561 (1991).
- <sup>8</sup> W. L. Roberts, J. F. Driscoll, M. C. Drake, and L. P. Goss, "Images of the quenching of a flame by vortex - to quantify regimes of turbulent combustion," *Combust. Flame* **94**, 58 (1993).
- <sup>9</sup> The reactant-product intermittency differs from internal or external intermittency of non-reacting turbulent flow, e.g., see V. R. Kuznetsov and V. A. Sabel'nikov, *Turbulence and Combustion* (Hemisphere Publ. Corp., New York, 1990).
- <sup>10</sup> K. N. C. Bray, P. A. Libby, and J. B. Moss, "Unified modeling approach for premixed turbulent combustion - Part I: General formulation," *Combust. Flame* **61**, 87 (1985).
- <sup>11</sup> K. N. C. Bray and J. B. Moss, "A unified statistical model for the premixed turbulent flame," *Acta Astronaut.* **4**, 291 (1977).
- <sup>12</sup> A. N. Lipatnikov, "Can we characterize turbulence in premixed flames?" *Combust. Flame* **156**, 1242 (2009).
- <sup>13</sup> A. N. Lipatnikov, "Conditioned moments in premixed turbulent reacting flows," *Proc. Combust. Inst.* **33**, 1489 (2011).
- <sup>14</sup> For instance,  $\nabla \cdot \bar{\mathbf{u}}_t$  does not vanish in a constant-density flow in a general case, see P. A. Libby, "On the prediction of intermittent turbulent flows," *J. Fluid Mech.* **68**, 273 (1975).
- <sup>15</sup> R. Yu, A. N. Lipatnikov, and X.-S. Bai, "Three-dimensional direct numerical simulation study of conditioned moments in turbulent reacting flows," *Phys. Fluids* **26**, 085104 (2014).
- <sup>16</sup> A. M. Steinberg, J. F. Driscoll, and S. L. Ceccio, "Measurements of turbulent premixed flame dynamics using cinema stereoscopic PIV," *Exp. Fluids* **44**, 985 (2008).
- <sup>17</sup> A. M. Steinberg and J. F. Driscoll, "Straining and wrinkling processes during turbulence-premixed flame interaction measured using temporally-resolved diagnostics," *Combust. Flame* **156**, 2285 (2009).
- <sup>18</sup> A. M. Steinberg, J. F. Driscoll, and S. L. Ceccio, "Three-dimensional temporally resolved measurements of turbulence-flame interactions using orthogonal-plane cinema-stereoscopic PIV," *Exp. Fluids* **47**, 527 (2009).
- <sup>19</sup> A. M. Steinberg, J. F. Driscoll, and S. L. Ceccio, "Temporal evolution of flame stretch due to turbulence and the hydrodynamic instability," *Proc. Combust. Inst.* **32**, 1713 (2009).
- <sup>20</sup> D. C. Haworth and T. J. Poinso, "Numerical simulations of Lewis number effects in turbulent premixed flames," *J. Fluid Mech.* **244**, 405 (1992).
- <sup>21</sup> M. Baum, T. J. Poinso, D. C. Haworth, and N. Darabiha, "Direct numerical simulation of H<sub>2</sub>/O<sub>2</sub>/N<sub>2</sub> flames with complex chemistry in two-dimensional turbulent flows," *J. Fluid Mech.* **281**, 1 (1994).
- <sup>22</sup> T. Echekki and J. H. Chen, "Unsteady strain rate and curvature effects in turbulent premixed methane-air flames," *Combust. Flame* **106**, 184 (1996).

- <sup>23</sup> D. Veynante and T. Poinso, "Effects of pressure gradients on turbulent premixed flames," *J. Fluid Mech.* **353**, 83 (1997).
- <sup>24</sup> J. H. Chen, T. Echehki, and W. Kollmann, "The mechanism of two dimensional pocket formation in lean premixed methane-air flames with implications to turbulent combustion," *Combust. Flame* **116**, 15 (1999).
- <sup>25</sup> M. Tanahashi, M. Fujimura, and T. Miyauchi, "Coherent fine-scale eddies in turbulent premixed flames," *Proc. Combust. Inst.* **28**, 529 (2000).
- <sup>26</sup> D. Thévenin, O. Gicquel, J. de Charentenay, R. Hilbert, and D. Veynante, "Two- versus three-dimensional direct simulations of turbulent methane flame kernels using realistic chemistry," *Proc. Combust. Inst.* **29**, 2031 (2002).
- <sup>27</sup> Y. Nada, M. Tanahashi, and T. Miyauchi, "Effect of turbulence characteristics on local flame structure of H<sub>2</sub>-air premixed flames," *J. Turbul.* **6**, 16 (2004).
- <sup>28</sup> S. Nishiki, T. Hasegawa, R. Borghi, and R. Himeno, "Modelling of turbulent scalar flux in turbulent premixed flames based on DNS databases," *Combust. Theory Modell.* **10**, 39 (2006).
- <sup>29</sup> Y. Shim, S. Tanaka, M. Tanahashi, and T. Miyauchi, "Local structure and fractal characteristics of H<sub>2</sub>-air turbulent premixed flame," *Proc. Combust. Inst.* **33**, 1455 (2011).
- <sup>30</sup> N. Chakraborty and A. N. Lipatnikov, "Effects of Lewis number on conditional fluid velocity statistics in low Damköhler number turbulent premixed combustion: A direct numerical simulation analysis," *Phys. Fluids* **25**, 045101 (2013).
- <sup>31</sup> T. C. Treurniet, F. T. M. Nieuwstadt, and B. J. Boersma, "Direct numerical simulation of homogeneous turbulence in combination with premixed combustion at low Mach number modelled by the *G*-equation," *J. Fluid Mech.* **565**, 25 (2006).
- <sup>32</sup> P. E. Hamlington, A. Y. Poludnenko, and E. S. Oran, "Interactions between turbulence and flames in premixed reacting flows," *Phys. Fluids* **23**, 125111 (2011).
- <sup>33</sup> P. E. Hamlington, A. Y. Poludnenko, and E. S. Oran, "Intermittency in premixed turbulent reacting flows," *Phys. Fluids* **24**, 075111 (2012).
- <sup>34</sup> N. Chakraborty, "Statistics of vorticity alignment with local strain rates in turbulent premixed flames," *Eur. J. Mech. B/Fluids* **46**, 201 (2014).
- <sup>35</sup> M. S. Uberoi, A. M. Kuethe, and H. R. Menkes, "Flow field of a Bunsen flame," *Phys. Fluids* **1**, 150 (1958).
- <sup>36</sup> S. Nishiki, T. Hasegawa, R. Borghi, and R. Himeno, "Modeling of flame-generated turbulence based on direct numerical simulation databases," *Proc. Combust. Inst.* **29**, 2017 (2002).
- <sup>37</sup> Y. H. Im, K. Y. Huh, S. Nishiki, and T. Hasegawa, "Zone conditional assessment of flame-generated turbulence with DNS database of a turbulent premixed flame," *Combust. Flame* **137**, 478 (2004).
- <sup>38</sup> A. Mura, K. Tsuboi, and T. Hasegawa, "Modelling of the correlation between velocity and reactive scalar gradients in turbulent premixed flames based on DNS data," *Combust. Theory Modell.* **12**, 671 (2008).
- <sup>39</sup> A. Mura, V. Robin, M. Champion, and T. Hasegawa, "Small scale features of velocity and scalar fields in turbulent premixed flames," *Flow Turbul. Combust.* **82**, 339 (2009).
- <sup>40</sup> V. Robin, A. Mura, M. Champion, and T. Hasegawa, "Direct and indirect thermal expansion effects in turbulent premixed flames," *Combust. Sci. Technol.* **182**, 449 (2010).
- <sup>41</sup> V. Robin, A. Mura, and M. Champion, "Modeling of the effects of thermal expansion on scalar turbulent fluxes in turbulent premixed flames," *J. Fluid Mech.* **689**, 149 (2011).
- <sup>42</sup> K. N. C. Bray, M. Champion, P. A. Libby, and N. Swaminathan, "Scalar dissipation and mean reaction rates in premixed turbulent combustion," *Combust. Flame* **158**, 2017 (2011).
- <sup>43</sup> J. H. Chen, "Petascale direct numerical simulation of turbulent combustion - fundamental insights towards predictive models," *Proc. Combust. Inst.* **33**, 99 (2011).
- <sup>44</sup> A. J. Aspden, M. J. Day, and J. B. Bell, "Turbulence-flame interactions in lean premixed hydrogen: transition to the distributed burning regime," *J. Fluid Mech.* **680**, 287 (2011).
- <sup>45</sup> Y.-S. Shim, N. Fukushima, M. Shimura, Y. Nada, M. Tanahashi, and T. Miyauchi, "Radical fingering in turbulent premixed flame classified into thin reaction zones," *Proc. Combust. Inst.* **34**, 1383 (2013).
- <sup>46</sup> J. Schumacher, K. R. Sreenivasan, and V. Yakhot, "Asymptotic exponents from low-Reynolds-number flows," *New J. Phys.* **9**, 89 (2007).
- <sup>47</sup> N. Chakraborty, H. Kolla, R. Sankaran, E. R. Hawkes, J. H. Chen, and N. Swaminathan, "Determination of three-dimensional quantities related to scalar dissipation rate and its transport from two-dimensional measurements. Direct Numerical Simulation based validation," *Proc. Combust. Inst.* **34**, 1151 (2013).
- <sup>48</sup> J. B. Bell, M. S. Day, and M. J. Lijewski, "Simulation of nitrogen emissions in a premixed hydrogen flame stabilized on a low swirl burner," *Proc. Combust. Inst.* **34**, 1173 (2013).
- <sup>49</sup> T. D. Dunstan, Y. Minamoto, N. Chakraborty, and N. Swaminathan, "Scalar dissipation rate modelling for Large Eddy Simulation of turbulent premixed flames," *Proc. Combust. Inst.* **34**, 1193 (2013).
- <sup>50</sup> N. Chakraborty and A. N. Lipatnikov, "Conditional velocity statistics for high and low Damköhler number turbulent premixed combustion in the context of Reynolds Averaged Navier Stokes simulations," *Proc. Combust. Inst.* **34**, 1333 (2013).
- <sup>51</sup> N. Chakraborty and R. S. Cant, "Turbulent Reynolds number dependence of flame surface density transport in the context of Reynolds Averaged Navier Stokes simulations," *Proc. Combust. Inst.* **34**, 1347 (2013).
- <sup>52</sup> I. Yoshikawa, Y.-S. Shim, Y. Nada, M. Tanahashi, and T. Miyauchi, "A dynamic SGS combustion model based on fractal characteristics of turbulent premixed flames," *Proc. Combust. Inst.* **34**, 1373 (2013).
- <sup>53</sup> L. Wang, N. Chakraborty, and J. Zhang, "Streamline segment analysis of turbulent premixed flames," *Proc. Combust. Inst.* **34**, 1401 (2013).
- <sup>54</sup> The magnitudes of the mean terms  $\overline{T}_k$  are lower than the magnitudes of the counterpart conditioned terms  $\langle T_k|c \rangle$ , also because the probability of finding flamelets is substantially lower than unity in the present DNS.